AIAA JOURNAL
Vol. 44, No. 7, July 2006

Vibration and Large Deflection of Cantilevered Elastica Compressed by Angled Cable

David B. Holland,* Ilinca Stanciulescu,† and Lawrence N. Virgin‡
Duke University, Durham, North Carolina 27708
and
Raymond H. Plaut§
Virginia Polytechnic Institute and State University, Blacksburg, Virginia 24061

A thin cantilevered beam is compressed by a cable attached to the tip of the beam and terminating near the base. Large-deflection equilibrium configurations and small vibrations about equilibrium are investigated. This system has a direct application to solar-sail structures, where the structural booms could be designed to bend to supply tension loading in the sail membrane. The equilibrium and vibration properties are examined in three ways: numerical integration of the governing elastica equations using a shooting method, finite element analysis using ABAQUS, and experiments with a polycarbonate strip bent by a cable that is tightened with a turnbuckle. Equilibrium shapes and vibration mode shapes and frequencies are obtained for two different cable attachment points offset slightly from the beam's base in the axial and transverse directions. Frequencies obtained from a three-dimensional finite element analysis are also presented.

Nomenclature

a, b	=	offsets of the attachment point
E	=	modulus of elasticity
I	=	minimum moment of inertia
L	=	length of the beam
$M(s, t)$	=	bending moment
m	=	mass per unit length
P_{cr}	=	critical force for the system with no offsets
$P(t)$	=	tension in the cable
$P_v(s, t)$, $P_h(s, t)$	=	internal forces in the beam, vertical and horizontal components
s	=	arc length
t	=	time
$x(s, t)$, $y(s, t)$	=	coordinates of points on the beam axis
$\theta(s, t)$	=	rotation of the cross section of the beam
ω	=	circular frequency
$\omega_{1,P=k=0}$	=	fundamental natural frequency for a cantilever beam with no cable and no applied load

Subscripts

d	=	dynamic amplitude
e	=	equilibrium values

I. Introduction

ONE end of a cable is attached to the tip of a thin cantilevered beam, and the other end is attached to a point near the base of the beam (Fig. 1). The cable is then shortened, for example, by a turnbuckle, so that it compresses the beam and pulls the beam's tip in the direction of the cable's attachment point. If there is no offset, that is, if the cable is attached to the base of the beam, the beam remains straight until it reaches a buckling load that is four times higher than that for the case of an axial compressive load applied at the top of the beam.[1] If there is an offset, the beam begins to deflect as soon as the cable is shortened. Such a beam–cable configuration is related to the design of solar sails, in which a bent beam may be used to supply tension to the membrane.

Buckling and vibration of a cantilevered column subjected to a load that passes through a point on the column's axis, for example, the base, has been treated by various researchers. Critical loads were obtained analytically by Timoshenko and Gere[1] and experimentally by Willems.[2] Frequencies about the straight equilibrium configuration were computed by Huang et al.,[3] Anderson and Done,[4] Sugiyama et al.,[5] and Xiong et al.,[6] with experiments included in Refs. 3 and 6.

Postbuckled equilibrium shapes based on an elastica analysis were obtained by Mladenov and Sugiyama.[7] In Refs. 2–8 this problem was related to that of a column subjected to a tangential load at its tip, and Tabarrok and Xiong[8] discussed variational principles. Chaudhry and Rogers[9] used linear and nonlinear analyses to determine equilibrium shapes for the case in which there was no offset at the base, but the cable was attached eccentrically at the tip of the column. They were interested in the use of shape-memory-alloy actuators to control the shapes of beams. Tomski et al.[10] studied a related problem in which a rigid link was attached tangentially to the beam tip and passed through a fixed point on the beam axis. In that problem, the bending moment is not zero at the beam tip. In other related problems, a load that passes through a point on the column was considered in Ref. 8, and a cable passing through a point on the column and then through the base was analyzed in Ref. 10.

Two new features in the present study are the following: The end of the cable away from the beam tip is offset from the beam's axis, and vibrations about the deformed equilibrium states are investigated. Three approaches are utilized, and their results are compared. First, the beam is analyzed as an elastica and numerical solutions are obtained with a shooting method. The cable is treated as a stiff spring during vibrations. Next, ABAQUS is applied in a finite element analysis of the problem. Finally, experiments are conducted on a polycarbonate beam, with the use of a laser vibrometer to collect data. Equilibrium shapes and vibration frequencies and modes are presented and compared.

Received 2 June 2005; accepted for publication 10 January 2006.

*Graduate Research Assistant, Department of Mechanical Engineering and Materials Science. Student Member AIAA.
†Postdoctoral Research Associate, Department of Civil and Environmental Engineering. Member AIAA.
‡Professor, Department of Mechanical Engineering and Materials Science. Senior Member AIAA.
§D. H. Pletta Professor of Engineering, Charles E. Via Jr. Department of Civil and Environmental Engineering.

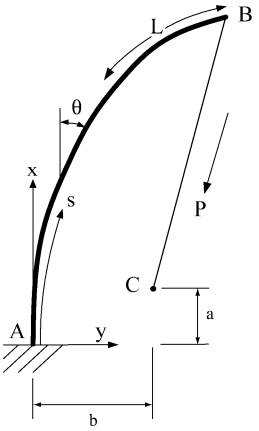

Fig. 1 Geometry of beam–cable system.

II. Numerical Modeling and Analysis

A. Analytical Elastica Model

1. General Formulation

Consider the system of a cantilever with a cable attached to its free end as shown in Fig. 1. The uniform beam is inextensible with length L, modulus of elasticity E, minimum moment of inertia I, that is, with respect to the plane of bending, and mass per unit length m. Points on the beam have coordinates $x(s,t)$ and $y(s,t)$. The rotation is denoted $\theta(s,t)$. The internal forces in the beam parallel to the $-x$ and $-y$ axes on a positive face, respectively, are $P_v(s,t)$ and $P_h(s,t)$. The beam is modeled as an elastica, with bending moment $M(s,t)$ proportional to the curvature.

The bottom of the cable is attached at point C in Fig. 1, which has coordinates $(x, y) = (a, b)$. (In the numerical results, a will be $0.0375L$ and b will be denoted the offset.) The cable remains straight, and the tension $P(t)$ in the cable has vertical component $P_v(L,t)$ and horizontal component $P_h(L,t)$ due to dynamic equilibrium at its upper end B. The cable is assumed to act as a spring with stiffness k.

Based on the geometry, moment-curvature relation, and dynamic equilibrium, and neglecting damping, the governing equations for the beam are

$$\frac{\partial x}{\partial s} = \cos\theta, \qquad \frac{\partial y}{\partial s} = \sin\theta, \qquad \frac{\partial \theta}{\partial s} = \frac{M}{EI}$$

$$\frac{\partial M}{\partial s} = P_h\cos\theta - P_v\sin\theta, \qquad \frac{\partial P_v}{\partial s} = -m\frac{\partial^2 x}{\partial t^2}$$

$$\frac{\partial P_h}{\partial s} = -m\frac{\partial^2 y}{\partial t^2} \tag{1}$$

The boundary conditions are

$$x(0,t) = 0, \qquad y(0,t) = 0, \qquad \theta(0,t) = 0$$

$$M(L,t) = 0, \qquad \frac{P_v(L,t)}{P_h(L,t)} = \frac{x(L,t)-a}{y(L,t)-b} \tag{2}$$

with the last one representing the condition that the cable remains straight.

2. Equilibrium Analysis

The subscript e is used to denote equilibrium values. In equilibrium, the internal force components P_{ve} and P_{he} are constant along the beam. Based on Eqs. (1), the variables $x_e(s)$, $y_e(s)$, $\theta_e(s)$, and $M_e(s)$ satisfy the equations

$$\frac{\mathrm{d}x_e}{\mathrm{d}s} = \cos\theta_e, \qquad \frac{\mathrm{d}y_e}{\mathrm{d}s} = \sin\theta_e, \qquad \frac{\mathrm{d}\theta_e}{\mathrm{d}s} = \frac{M_e}{EI}$$

$$\frac{\mathrm{d}M_e}{\mathrm{d}s} = P_{he}\cos\theta_e - P_{ve}\sin\theta_e \tag{3}$$

The associated boundary conditions are

$$x_e(0) = 0, \qquad y_e(0) = 0, \qquad \theta_e(0) = 0, \qquad M_e(L) = 0$$

$$P_{ve}/P_{he} = [x_e(L) - a]/[y_e(L) - b] \tag{4}$$

This boundary-value problem was solved numerically using a shooting method[11] in MATLAB®. The shear component P_{he} was specified, along with a, b, L, and EI. (The variables can be nondimensionalized such that L and EI are not involved in the code.) Equations (3) were solved as an initial-value problem, using the Runge–Kutta method with an assumed value of P_{ve}. The last condition in Eqs. (4) was replaced by

$$M_e(0) = P_{ve}b - P_{he}a \tag{5}$$

which was obtained using moment equilibrium about point A in Fig. 1, or by manipulation and integration in Eqs. (3) and (4). The parameter P_{ve} was updated, using Newton's method, until the condition $M_e(L) = 0$ was satisfied with sufficient accuracy.

3. Analysis of Small Vibrations About Equilibrium

Next, small vibrations about the equilibrium configurations are considered. The variables are written

$$x(s,t) = x_e(s) + x_d(s)\sin\omega t, \qquad y(s,t) = y_e(s) + y_d(s)\sin\omega t$$

$$\theta(s,t) = \theta_e(s) + \theta_d(s)\sin\omega t, \qquad M(s,t) = M_e(s) + M_d(s)\sin\omega t$$

$$P_v(s,t) = P_{ve} + P_{vd}(s)\sin\omega t, \qquad P_h(s,t) = P_{he} + P_{hd}(s)\sin\omega t \tag{6}$$

where d is a dynamic amplitude. Equations (6) are substituted into Eqs. (1) and (2), and the resulting equations are linearized in the dynamic variables.

The governing equations along the beam are found to be

$$\frac{\mathrm{d}x_d}{\mathrm{d}s} = -\theta_d\sin\theta_e, \qquad \frac{\mathrm{d}y_d}{\mathrm{d}s} = \theta_d\cos\theta_e, \qquad \frac{\mathrm{d}\theta_d}{\mathrm{d}s} = \frac{M_d}{EI}$$

$$\frac{\mathrm{d}M_d}{\mathrm{d}s} = P_{vd}\cos\theta_e - P_{hd}\sin\theta_e - \theta_d(P_{ve}\sin\theta_e + P_{he}\cos\theta_e)$$

$$\frac{\mathrm{d}P_{vd}}{\mathrm{d}s} = m\omega^2 x_d, \qquad \frac{\mathrm{d}P_{hd}}{\mathrm{d}s} = m\omega^2 y_d \tag{7}$$

The boundary conditions for the dynamic variables are

$$x_d(0) = 0, \qquad y_d(0) = 0, \qquad \theta_d(0) = 0, \qquad M_d(L) = 0 \tag{8}$$

plus the following conditions at $s = L$:

$$P_{vd}(y_e - b) + P_{ve}y_d = P_{hd}(x_e - a) + P_{he}x_d \tag{9}$$

$$\frac{P_{ve}P_{vd} + P_{he}P_{hd}}{\sqrt{P_{ve}^2 + P_{he}^2}} = \frac{k[(x_e - a)x_d + (y_e - b)y_d]}{\sqrt{(x_e - a)^2 + (y_e - b)^2}} \tag{10}$$

Equation (9) is obtained from the last condition in Eqs. (4), and Eq. (10) follows from the cable stiffness relation

$$\sqrt{P_h^2 + P_v^2} - \sqrt{P_{he}^2 + P_{ve}^2} = k\left(\sqrt{(x-a)^2 + (y-b)^2}\right.$$

$$\left. - \sqrt{(x_e - a)^2 + (y_e - b)^2}\right) \tag{11}$$

A similar shooting method was applied, using Eqs. (7–10), and also the equilibrium equations and their solutions, because equilibrium variables are involved in the dynamic boundary-value problem. The quantities a, b, L, EI, m, and k were specified. Because the vibration amplitude is arbitrary, the initial condition $M_d(0)$ could be specified, for example. The frequency ω and initial conditions $P_{vd}(0)$ and $P_{hd}(0)$ were updated until Eqs. (9) and (10) and the last condition in Eqs. (8) were satisfied. To obtain different frequencies and modes, the initial guess for ω was chosen in different ranges.

B. Finite Element Analysis

For the finite element simulations, the software ABAQUS[12] was utilized. The beam was discretized using first-order, shear-flexible (Timoshenko) three-dimensional beam elements (B31). These elements are formulated for large strains and large rotations, use linear interpolation, and allow for transverse shear strain, that is, the cross section does not necessarily remain normal to the beam centerline. However, whereas the axial strain can be arbitrarily large, due to some assumptions in the formulation, only a moderately large torsional strain is modeled accurately. In ABAQUS, this beam element is formulated to be efficient for thin beams (for which the Euler–Bernoulli theory is accurate) as well as thick beams.

The discretization of the beam has 1000 such elements, which was sufficient for the desired accuracy in both the static and the dynamic calculations (as was confirmed by a spatial convergence study). The material and geometrical properties utilized for the beam were consistent with the values used in the shooting method, were measured experimentally where possible, and will be introduced in the following section. The cable was assumed to deform only by axial stretching and was modeled with a single two-node, linear interpolation truss element (T3D2) having three degrees of freedom per node. Because of the intrinsic restrictions of any finite element simulation, to apply a load that strictly follows the direction of the cable, the material of the cable was defined to be temperature sensitive and the desired axial load was applied indirectly via a change in temperature.

III. Experimental Verification

A. Experimental Hardware and Instrumentation

To verify the numerical analysis and results, experiments were performed using a simple beam and cable configuration. The test specimen was a slender, prismatic, polycarbonate beam mounted horizontally with one end clamped, as shown in Fig. 2a. The dimensions of the beam and material were chosen to minimize the effect of gravity on the resulting deflection and natural frequencies. The beam specimen had the following dimensions: length 0.762 m, height 25.4 mm, and thickness 4.8 mm. The beam material was molded polycarbonate with a modulus of 1.656 GPa and density of 1120 kg/m^3.

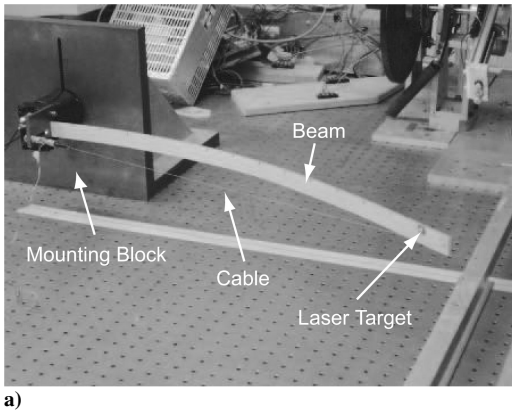

a)

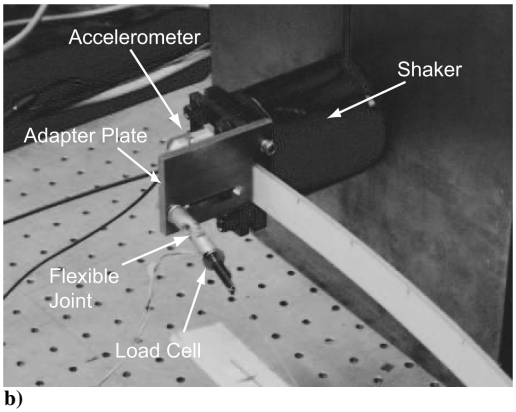

b)

Fig. 2 Beam–cable system experimental hardware and mounting.

Initial experiments and analyses were performed on a steel beam with similar dimensions to the polycarbonate beam. However, it was impossible to generate highly deflected static shapes without permanently deforming the test sample. For this reason, the polycarbonate material was chosen for its high flexibility and became the focus for the static and dynamic studies.

The free end of the beam was attached to a cable capable of handling many times the critical buckling load before yielding. The wire was a woven steel cable with a breaking strength of 240 N. Tensile testing was performed on the cable to determine the approximate spring stiffness of the cable, 11.67 kN/m.

Two steel plates were bolted together using four bolts with the polycarbonate beam clamped tightly between them. An adapter plate was mounted to the side to allow the attachment point of the cable to be changed. However, sufficient clearance between the adapter plate and the beam ensured that the base hardware did not interfere with either the static deflection or the dynamic measurements of the system. A flexible joint was attached to the adapter plate, and the cable was attached to the free end of the joint. Figure 2b shows a closeup view of the mounting hardware.

To measure the tension in the cable at various load levels, a miniature load cell, also visible in Fig. 2b, was placed between the free end of the flexible joint and the cable. This made direct tension measurement of the cable possible. The load cell was powered by a dc power supply, and the output voltage (read using a multimeter) was later converted to tension measurements.

To capture dynamic behavior of the beam and cable system, three experimental components were used. First, an accelerometer, visible in Fig. 2b, was attached to the clamping base of the setup to capture dynamic input to the beam. The clamping base of the structure was then bolted to a small-amplitude (4-mm) shaker. The shaker was bolted on a 50-kg steel mounting bracket, which was itself bolted to a vibration isolation table. A point-to-point laser vibrometer, mounted horizontally 1 m away from the test article, was used to capture dynamic measurements at a target point near the end of the beam. A Brüel and Kjaer data acquisition system was used to control the dynamic testing as well as drive the shaker and collect the dynamic data from the accelerometer and laser vibrometer.

B. Experimental Procedure

Experimental trials consisted of static deflection measurements, small-amplitude vibration measurements, and sample modal analysis measurements. For the first two, a quick but repeatable procedure was developed. First, the cable was shortened and tied off near the load cell to change the loading and deflection in the beam. Load measurements were then taken from the miniature load cell. Following that, a static deflection measurement was taken by measuring the tip deflection of the beam. Then the frequency measurement data were collected using the data acquisition system. Following the dynamic trial, a repeat measurement of the static deflection and cable tension was performed to ensure that no gross change occurred in the system during the dynamic data collection, for example, beam slippage, cable slippage, or hardware motion.

A standard set of parameters was used in the collection of the beam vibrational data. The shaker was excited with a pseudorandom input signal with frequency content from 0 to 100 Hz. A delay of 5 s between the start of the shaker and the beginning of data collection was used to allow transient motions to dampen. Fast Fouier transform (FFT) data were collected from the accelerometer and laser vibrometer using 3200 lines between 0 and 100 Hz, for a Δf of 0.03125 Hz. For each load level, six averages were taken using 50% data overlap and Hanning windowing on both the laser and accelerometer data. The natural frequencies were then estimated from the peaks of the H3 frequency response (root-mean-squared transfer function) using the laser as the signal and the accelerometer as the reference. An example of the frequency-response data is shown in Fig. 3a. The value P_{cr} in the caption will be defined in the following section. Experimental static and dynamic data were collected for multiple static configurations, using $a = 28.6$ mm (which

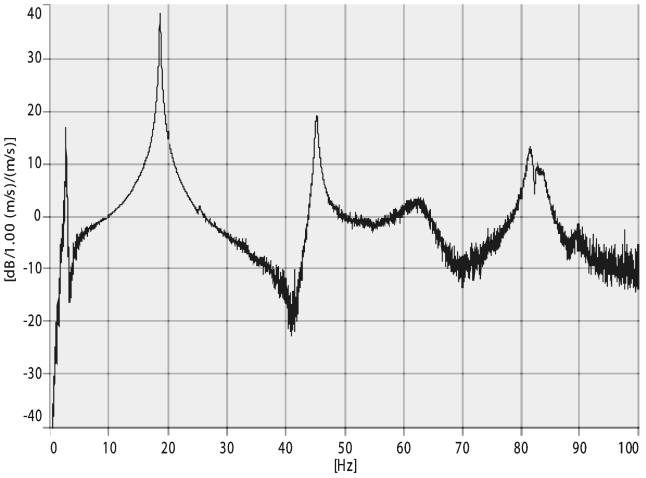

a) H3 frequency response function ($P/P_{cr} = 1.12$, $b/L = 0.0167$)

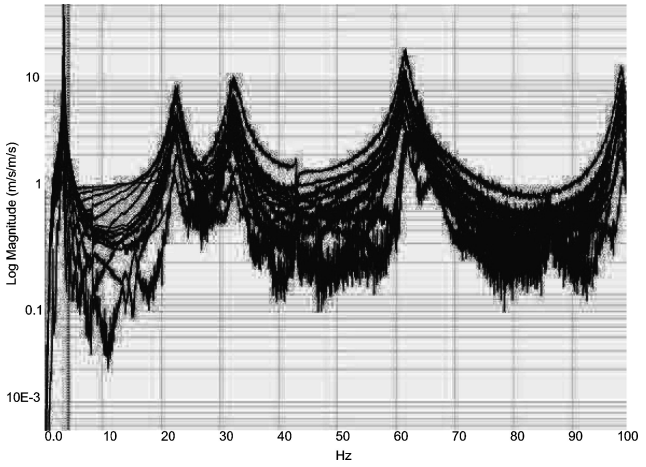

b) Overlaid frequency response functions for modal analysis ($P/P_{cr} = 0.505$, $b/L = 0.0750$)

Fig. 3 Sample experimental data.

is the value that is used for this parameter in all of the following examples) and two b values, 12.7 and 57.1 mm. When normalized with respect to the length of the beam, these offset values translate to approximately $a/L = 0.0375$, $b/L = 0.0167$, and $b/L = 0.0750$, respectively.

An experimental modal analysis was also performed at a particular configuration of the loaded beam and cable. For the modal analysis, dynamic data were collected at 15 equidistant points along the length of the beam. The first four mode shapes were then estimated using the ME'Scope modal analysis program. Figure 3b shows the 15 frequency responses overlaid.

IV. Comparison and Analysis of Results

A. Static Analysis

If the cable passes through the base of the cantilevered beam and the tension in the cable is increased, the beam remains straight until buckling occurs when P reaches the critical value[1]

$$P_{cr} = \pi^2 EI/L^2 \tag{12}$$

As the beam begins to buckle, the moment at the base (as well as at the tip) is zero, and so the effective length is L as for a pinned–pinned column. If the load were to act vertically instead of passing through the base, the effective length would be $2L$ and the critical load would be one-fourth the value in Eq. (12). In both cases the loading is conservative.

As stated before, $a = 0.0375L$ in the experiments and all of the numerical results. Figure 4 shows a sequence of equilibrium configurations for the offset $b/L = 0.0167$ as P is increased. The beam bends as soon as the cable tension is nonzero.

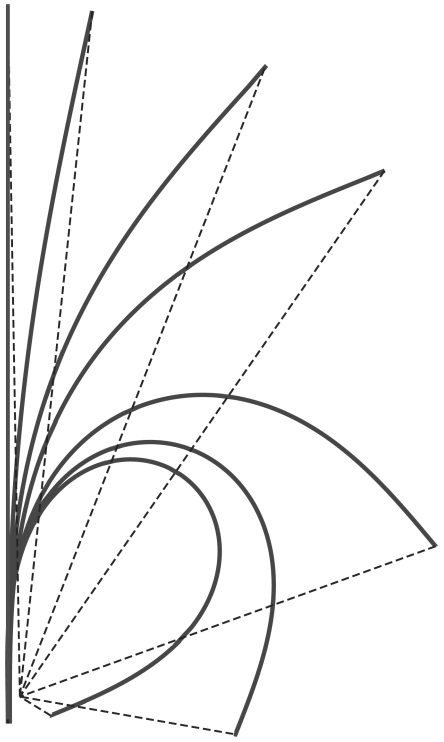

Fig. 4 Equilibrium shapes for $b/L = 0.0167$ and $P/P_{cr} = 0.81$, 1.01, 1.08, 1.30, 1.66, and 2.2.

Figures 5a and 5b show equilibrium paths for offsets $b/L = 0.0167$ and 0.075, respectively. The abscissa is the normalized horizontal deflection at the tip of the beam. Experimental values are denoted by open squares, numerical solutions from the elastica analysis are shown as continuous curves, and results from the finite element analysis are given by the dashed curves. Good agreement is observed, with a better match exhibited for the case with a larger offset (Fig. 5b).

In Fig. 6, additional results from the finite element analysis are drawn. The offsets used are $b/L = 0.0131$, 0.0263, 0.0394, and 0.0525. The maximum tip deflection decreases as the offset increases.

B. Small Vibrations About Equilibrium

The first four frequencies for small vibrations about the equilibrium configuration are plotted in Fig. 7 for offset $b/L = 0.0167$ and cable stiffness $k = 11.67$ kN/m. The frequency is normalized by the fundamental natural frequency $3.516/L^2\sqrt{(EI/m)}$ of a cantilever with no cable and no applied load, k and $P = 0$. Again, the continuous curves correspond to the elastica analysis, the dashed curves to finite element results, and the open squares to experimental data. The data in Fig. 3a correspond to experimental points in Fig. 7 at $P/P_{cr} = 1.12$.

The results for the fundamental frequency ω_1 are shown in Fig. 8 with a magnified frequency axis. As the tension in the cable is increased past $P = P_{cr}$, the fundamental frequency tends to decrease and then increase, whereas the other frequencies in Fig. 7 tend to do the opposite.

Similar results for offset $b/L = 0.075$ are presented in Figs. 9 and 10. For this larger offset, the frequencies shown are higher for low values of tension and then become comparable to those for the lower offset. Again, when P is near P_{cr} the fundamental frequency exhibits a minimum and each of the next three frequencies exhibits a maximum. The data in Fig. 3b correspond to experimental points in Fig. 9 at $P/P_{cr} = 0.505$.

For the offset $b/L = 0.075$, vibration modes are shown in Figs. 11 and 12, with the equilibrium shape of the beam also shown. Figure 11 shows the first four modes obtained from the elastica analysis. Except for the second mode, the tip of the beam sways considerably

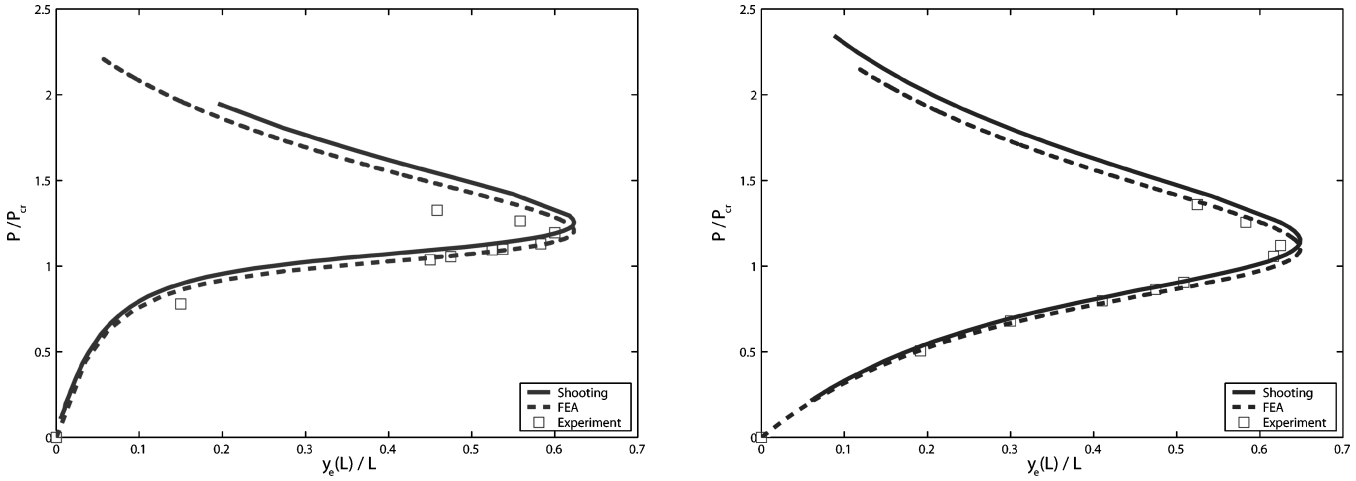

a) $b/L = 0.0167$ **b) $b/L = 0.0750$**

Fig. 5 Tension vs horizontal tip deflection for two offsets.

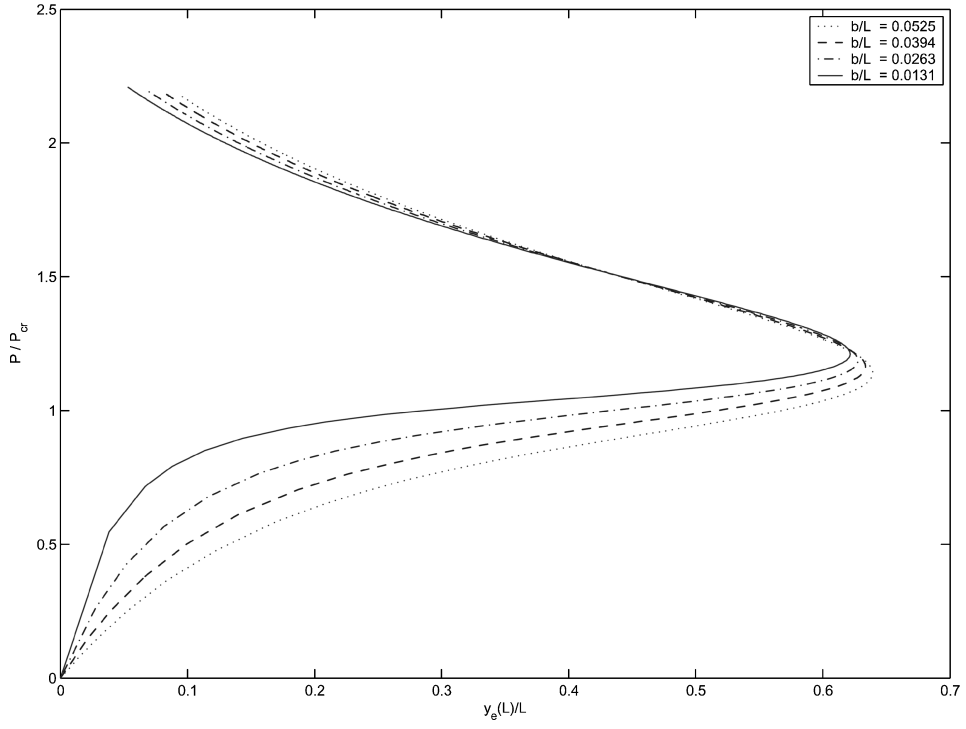

Fig. 6 Tension vs horizontal tip deflection for four offsets.

during vibration. A comparison of the fourth mode obtained from finite element analysis (FEA) (Fig. 12a), elastica analysis (Fig. 12b), and experiments (Fig. 12c) is seen in Fig. 12. The correlation between the results is good.

Finally, a full three-dimensional FEA was conducted using ABAQUS. The bending stiffness of the beam was 30 times greater in the strong direction than in the weak direction. However, the out-of-plane modes appeared quite early in the mode sequence, especially for larger axial loads. This can be explained by the additional constraint imposed by the cable in the plane in which most of the deformation occurs. This constraint increases the structural stiffness in that plane. Figure 13 presents results from the three-dimensional analysis for offset $b/L = 0.0167$. The larger dots are associated with out-of-plane modes. As the cable tension is increased from zero, the corresponding frequencies tend to decrease, and the second and third of these sets of frequencies intersect curves associated with in-plane modes. At high loads, frequencies for in-plane and out-of-plane vibration modes alternate in Fig. 13.

C. Discrepancies and Measurement Errors

In general, we obtained a good agreement between different sets of results. As an example, we show in Fig. 14 the percentile differences in the results for the fundamental mode. (The FE results are taken as reference, and differences are shown between those and the experimental and analytical results.) It can be seen that the difference between FE results and results obtained by numerical integration of the elastica equations is less than 5% in all cases, whereas the deviation of the experimental results is $\sim$20% for the small offset and $\sim$40% for the large one. This deviation increases with the lateral offset and with the axial load.

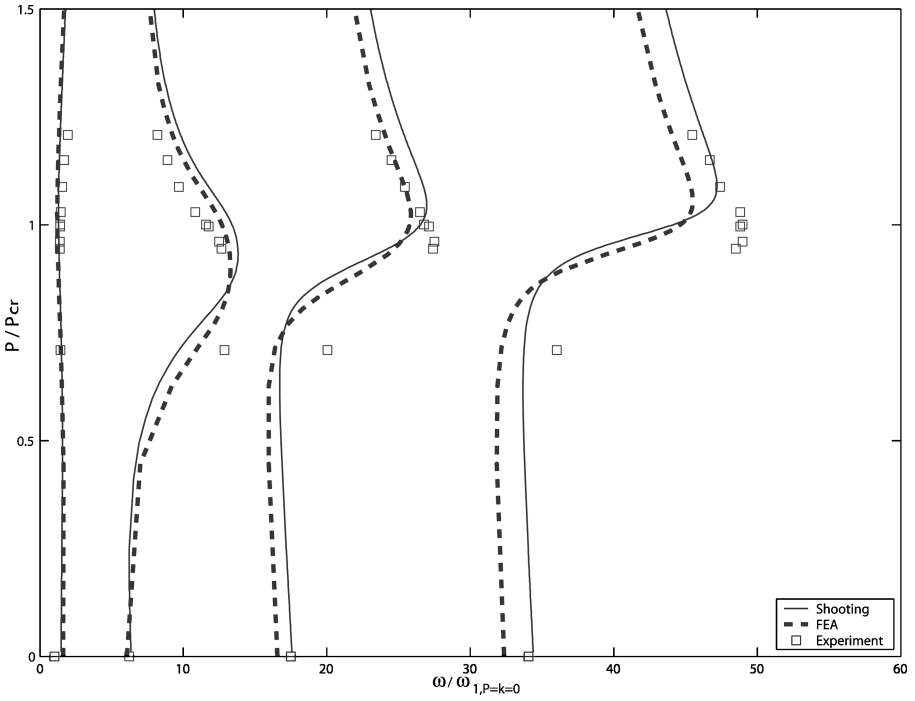

Fig. 7 Lowest four frequencies for $b/L = 0.0167$.

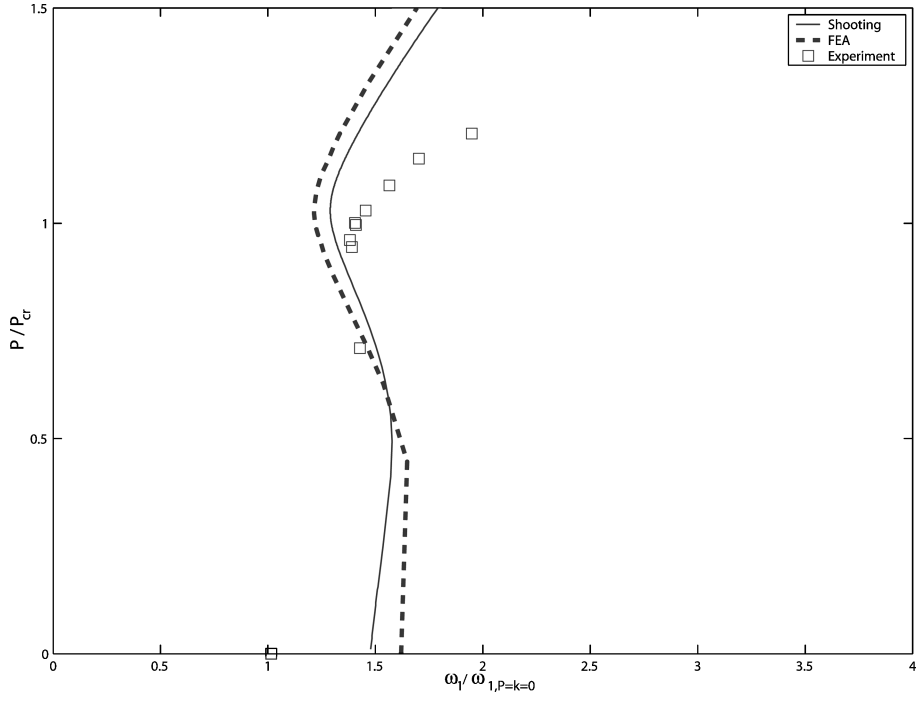

Fig. 8 Fundamental frequency for $b/L = 0.0167$.

When the FE approach is used, analyses are performed using the software ABAQUS, and first-order, three-dimensional Timoshenko (shear-flexible) beam elements (B31) are used for discretization. These elements are formulated for large strains and large rotations, allow for transverse shear deformation, and are efficient for thick as well as slender beams. The discretizations utilized are proved (via a spatial convergence study) to offer the desired accuracy. A spatial convergence study performed exposed a surprising effect: The number of elements required in the dynamic analysis is much larger than what proves to be more than sufficient in the case of the static analysis. All results presented in this paper are obtained based on these very refined discretizations. The results obtained using the shooting method to integrate the elastica equations do not include effects from shear or axial deformation, and this is one of the possible causes of the differences observed in the results.

In addition, some uncertainties affect the experimental data. We estimate a 5% precision error in the experimental load measurement and a 1% error in the measurement of the deflection. The natural frequency should be accurate to within 1% based on the method used to take the data and the number of averages used.

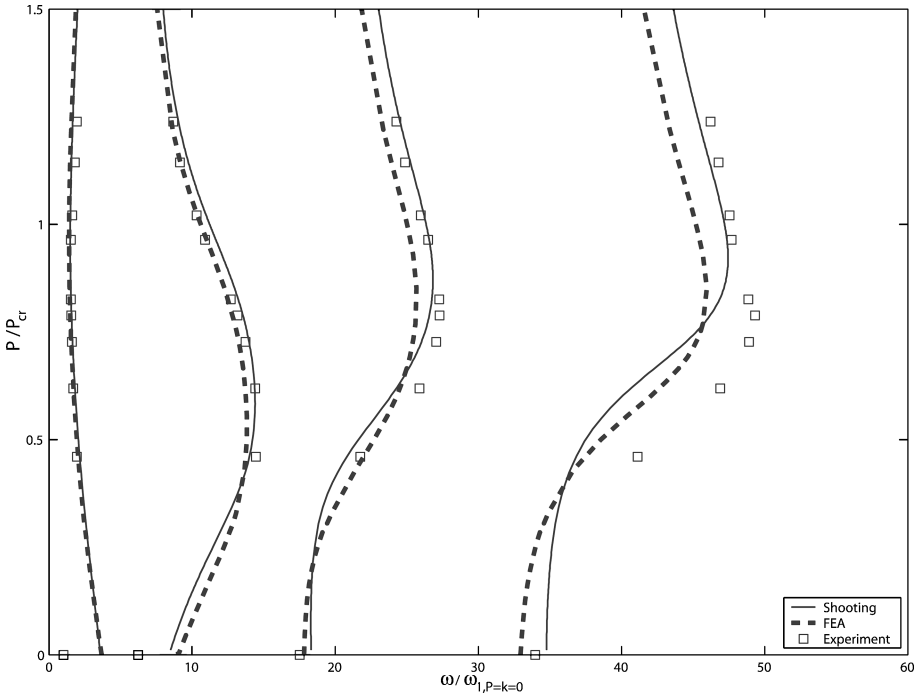

Fig. 9 Lowest four frequencies for $b/L = 0.0750$.

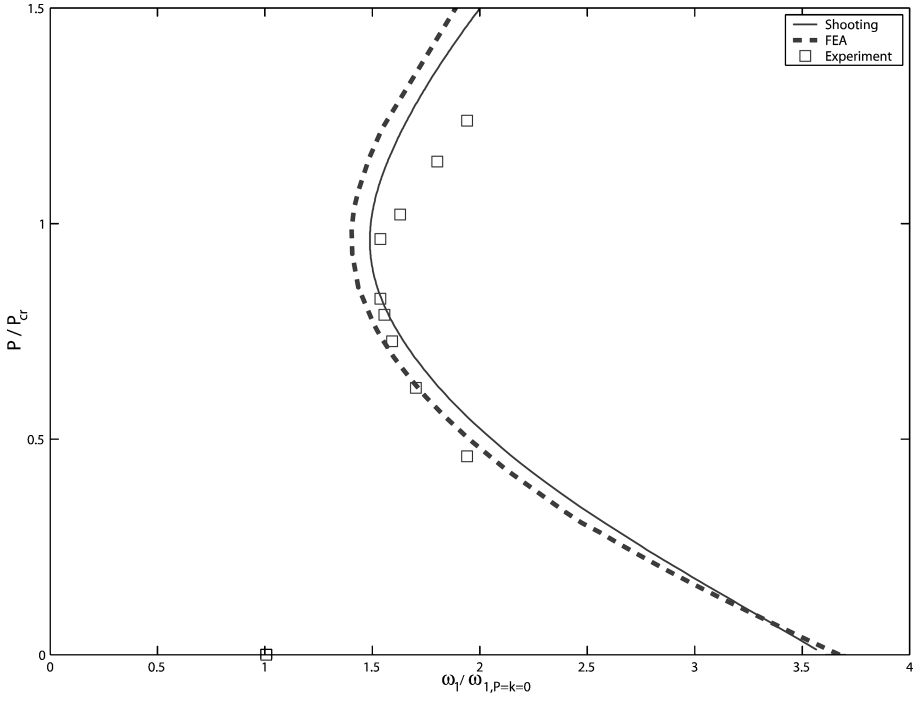

Fig. 10 Fundamental frequency for $b/L = 0.0750$.

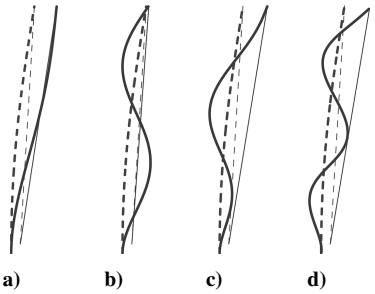

Fig. 11 First four vibration modes for $b/L = 0.0750$ and $P/P_{cr} = 0.505$ from shooting.

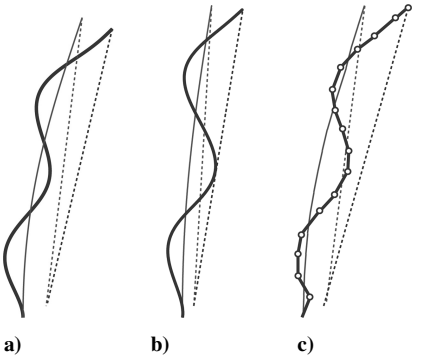

Fig. 12 Fourth vibration mode for $b/L = 0.0750$ and $P/P_{cr} = 0.505$ for a) FEA, b) shooting, and c) experiments.

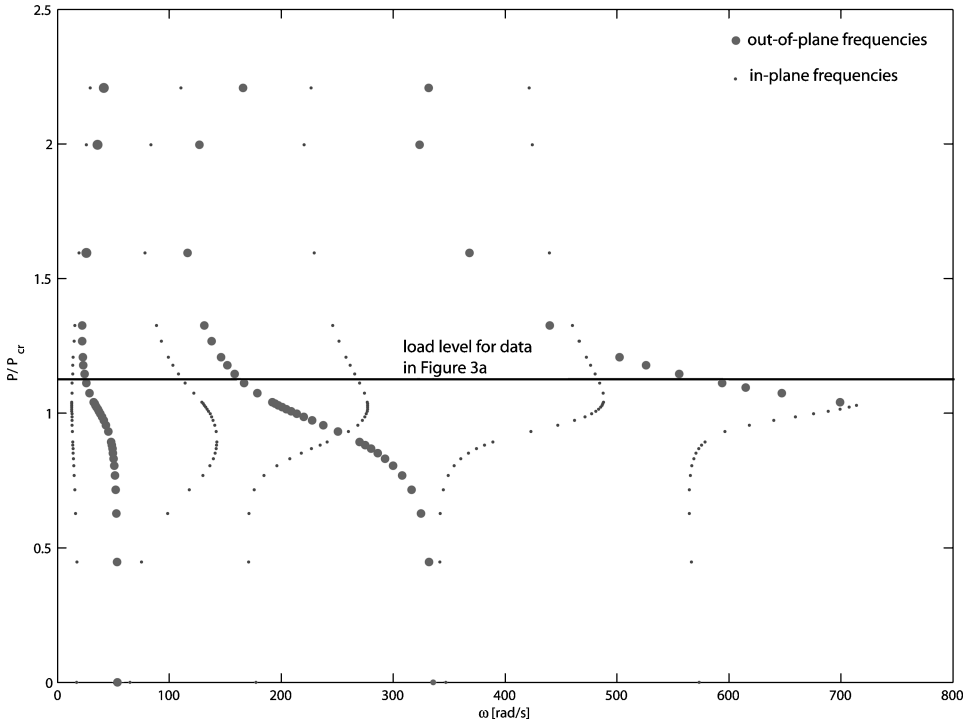

Fig. 13 Frequencies for $b/L = 0.0167$ from three-dimensional FEA.

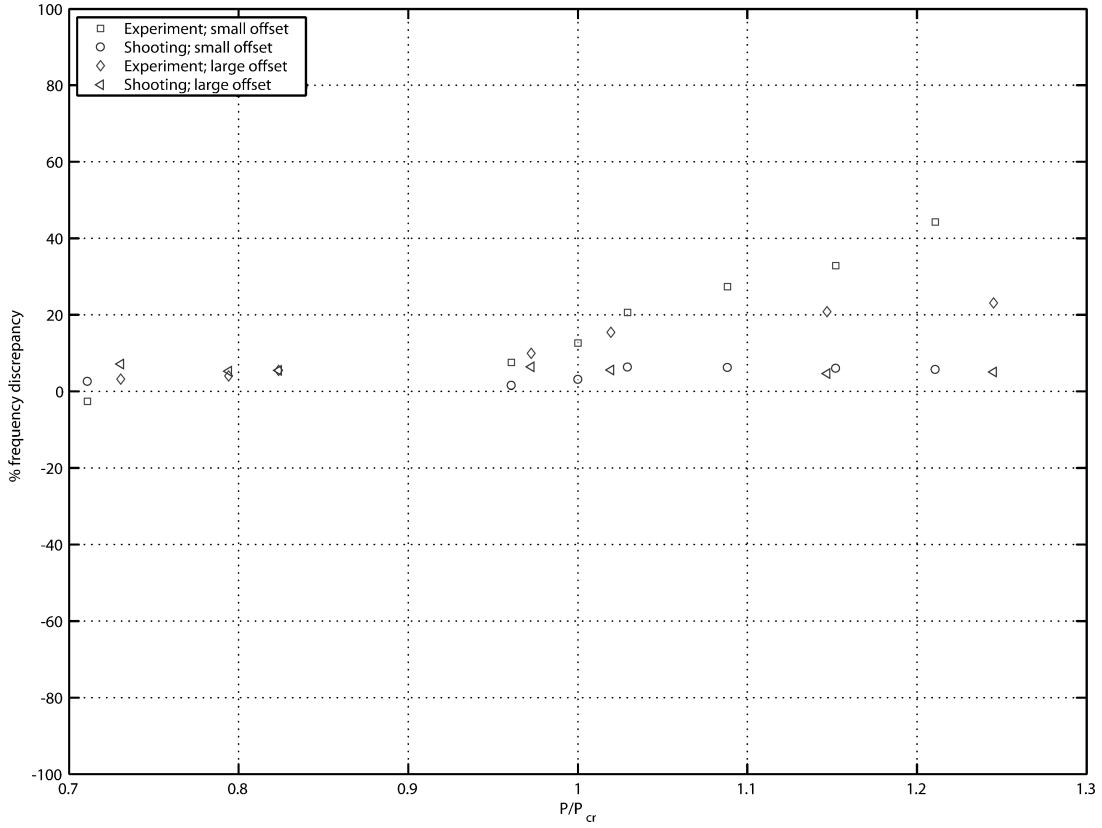

Fig. 14 Discrepancies between sets of results.

V. Conclusions

This study was motivated by solar-sail structures in which a boom could be buckled to provide tension to the sail. Two-dimensional large deflections of a cantilevered beam were considered. A cable connecting the tip of the beam and a point near the beam's base was tightened, which compressed and bent the beam. Equilibrium configurations and small vibrations about them were analyzed with three approaches: an elastica analysis, FEA, and experiments with a thin polycarbonate strip. The results demonstrated good correlation among the three methods. The elastica and FEA assumed two-dimensional vibrations, a massless cable, no damping, and no gravitational effects. These are idealizations of the behavior in the experiments, of course, and may account for some of the minor differences observed in the figures.

If there were no offset, the cable would line up with the straight beam and buckling would occur at a load P_{cr} that is four times greater

than that for a cantilever under a load that acts in an axial direction during postbuckling. For the angled cable treated here, deflections occur as soon as the cable is tightened. Deflections are larger for a larger transverse offset until the load approaches the value P_{cr}, as is usual for compressed structures with imperfections.

Loads greater than twice P_{cr} were considered, with the beam almost forming a loop. The first vibration frequency tends to exhibit a minimum as the load passes P_{cr}, whereas the next three tend to exhibit a maximum. For large loads, out-of-plane modes may have surprisingly low frequencies, due partly to the reduced constraint caused by the cable for those motions.

In the FEA, the load was applied indirectly via a temperature variation. This was necessary to make sure that the direction of the load (always following the direction of the cable) is preserved. In some sense this is also helpful numerically: It has the advantage of creating a path-following procedure that is neither force controlled nor displacement controlled, but rather an indirect arc-length approach, which in itself is more stable and appropriate for path following in problems with bifurcations and critical points along the path.

Acknowledgments

The first author acknowledges the support of the NASA Graduate Student Research Program. The fourth author acknowledges the support of the National Science Foundation under Grant 0114709.

References

[1]Timoshenko, S. P., and Gere, J. M., *Theory of Elastic Stability*, 2nd ed., McGraw–Hill, New York, 1961, pp. 55–57.

[2]Willems, N., "Experimental Verification of the Dynamic Stability of a Tangentially Loaded Cantilever Column," *Journal of Applied Mechanics*, Vol. 33, No. 2, 1966, pp. 460–461.

[3]Huang, N. C., Nachbar, W., and Nemat-Nasser, S., "On Willems' Experimental Verification of the Critical Load in Beck's Problem," *Journal of Applied Mechanics*, Vol. 34, No. 1, 1967, pp. 243–245.

[4]Anderson, N. A., and Done, G. T. S., "On the Partial Simulation of a Nonconservative System by a Conservative System," *International Journal of Solids and Structures*, Vol. 7, No. 1, 1971, pp. 183–191.

[5]Sugiyama, Y., Mladenov, K. A., and Fusayasu, K., "Stability and Vibration of Elastic Systems Subjected to a Central Force," Faculty of Engineering, Repts. 14/1, Tottori Univ., Tottori City, Japan, Oct. 1983.

[6]Xiong, Y., Wang, T. K., and Tabarrok, B., "On a Centripetally Loaded Model Simulating Beck's Column," *International Journal of Solids and Structures*, Vol. 25, No. 10, 1989, pp. 1107–1113.

[7]Mladenov, K. A., and Sugiyama, Y., "Buckling of Elastic Cantilevers Subjected to a Polar Force: Exact Solution," *Transactions of the Japan Society for Aeronautical and Space Sciences*, Vol. 26, No. 72, 1983, pp. 80–90.

[8]Tabarrok, B., and Xiong, Y., "A New Perspective on Variational Methods for Stability Analysis of Columns," *Acta Mechanica*, Vol. 78, No. 3–4, 1989, pp. 191–207.

[9]Chaudhry, Z., and Rogers, C. A., "Bending and Shape Control of Beams Using SMA Actuators," *Journal of Intelligent Material Systems and Structures*, Vol. 29, No. 20, 1992, pp. 581–602.

[10]Tomski, L., Przybylski, J., Golebiowska-Rozanow, M., and Szmidla, J., "Vibration and Stability of a Cantilever Column Subjected to a Follower Force Passing Through a Fixed Point," *Journal of Sound and Vibration*, Vol. 214, No. 1, 1998, pp. 67–81.

[11]Burden, R. L., and Faires, J. D., *Numerical Analysis*, 6th ed., Brooks/Cole, Pacific Grove, CA, 1997, Chap. 11, pp. 632–639.

[12]*ABAQUS Analysis User's Manual*, Ver. 6.4, ABAQUS, Inc., Providence, RI, 2003.

E. Livne
Associate Editor